Evaluation of the fatigue properties for the long-term service asphalt pavement using the semi-circular bending tests and stereo digital image correlation technique

Cheng, Long; Zhang, Lei ; Liu, Xueyan; Yuan, Fang ; Ma, Yang; Sun, Yinqing

DOI
10.1016/j.conbuildmat.2021.126119

Publication date
2022

Document Version
Final published version

Published in
Construction and Building Materials

Construction and Building Materials 317 (2022) 126119

Contents lists available at ScienceDirect

Construction and Building Materials

journal homepage: www.elsevier.com/locate/conbuildmat

Evaluation of the fatigue properties for the long-term service asphalt pavement using the semi-circular bending tests and stereo digital image correlation technique

Long Cheng [a,d], Lei Zhang [a,*], Xueyan Liu [b,*], Fang Yuan [c], Yang Ma [d], Yinqing Sun [a,d]

[a] Intelligent Transportation System Research Center of Southeast University, Nanjing 210096, China
[b] Section of Pavement Engineering, Faculty of Civil Engineering and Geosciences, Delft University of Technology, Delft, The Netherlands
[c] School of Civil Engineering, Southeast University, Nanjing 210096, China
[d] School of Transportation, Southeast University, Nanjing 210096, China

ARTICLE INFO

Keywords:
Fatigue performance
SCB test
K-d tree algorithm
CZM
Paris law

ABSTRACT

Reliable assessment of the fatigue resistance of asphalt pavement with a long-term service is critically crucial for the rational formulation of original pavement utilization strategies in reconstruction and expansion projects. Currently, the pavement performance evaluation indicators are mainly used to guide pavement preventive maintenance, and its applicability in reconstruction and expansion projects of the freeway is limited. This paper aims to propose an evaluation method of fatigue resistance of asphalt concrete utilizing semi-circular bending (SCB) tests and stereo digital image correlation (stereo-DIC) techniques. A total of 27 asphalt concrete cores were drilled from the three freeways (K84, K124, and K165) with a service life of more than 20 years, and the SCB specimens were produced to conduct the SCB fracture and fatigue tests. During the SCB test, the stereo-DIC technique was employed to monitor the evolution process of the strain distribution and crack length for the specimens. K-dimension tree neighbor-searching algorithm (K-d tree algorithm) was used to effectively measure the change of crack length corresponding to each fatigue load cycle. Meanwhile, the strain threshold of asphalt concrete crack initiation was determined by the bilinear softening cohesive zone model (CZM) to ensure the accuracy of the crack length calculated by the K-d tree algorithm. Furthermore, the relationship between crack growth rate and stress intensity, which was used to fit the Paris law parameters, was determined. The CZM and DIC results indicated that the strain threshold of asphalt concrete crack should be set as 2000 $\mu\varepsilon$ when using the K-d tree algorithm to determine the crack length. With the stress ratio increase, the Paris law parameter A increased wavily, and the parameter n decreased steadily, while the threshold of the stress intensity factor increased steadily. The Paris law master curves could characterize the fatigue performance of various road sections at a wide load range. The residual fatigue life of K84, K124, K165 the road sections were 2.13E + 08, 3.57E + 08, and 1.02E + 07, respectively.

1. Introduction

In the past two decades, with the rapid economic development, the traffic volume also increased dramatically, which led to the accelerated aging and deterioration of the highway system in all countries around the world [1,2]. For instance, the high-performance asphalt concrete freeways of China were extensively constructed around 2000, while the design benchmark period (typically 15 years) for hot mix asphalt (HMA) pavement was relatively short. Most of the high-performance freeways in China are now approaching or beyond their design service life, which means that freeways reconstruction and expansion treatments should be conducted to ensure the service level of the pavement [3]. For the reconstruction and expansion project, rational utilization of the original pavement structure is of great significance to reduce the economic cost and the consumption of natural resources and carbon emissions. Therefore, a comprehensive evaluation of fatigue resistance and residual life of asphalt concrete is of great importance to determine the utilizing strategies (milling depths, pavement resurfacing thickness, etc.) for the original asphalt surface layer.

Several laboratory test methods were used to characterize the fatigue

* Corresponding authors.
E-mail addresses: zhanglei1905seu@163.com (L. Zhang), x.liu@tudelft.nl (X. Liu).

https://doi.org/10.1016/j.conbuildmat.2021.126119
Received 6 July 2021; Received in revised form 9 December 2021; Accepted 14 December 2021
Available online 30 December 2021

properties of asphalt concrete, including indirect tensile test (IDT), overlay test (OT), direct tensile test (DT), and four-point bending beam fatigue (FBBF) tests [4–8]. In contrast, the semi-circular bending (SCB) fatigue test has the following advantages [9–11]: (a) specimen preparation is easy and the field core samples can be used directly, (b) the stress distribution in the specimen is similar to the actual stress state of the field pavement structure, (c) the fatigue crack propagation, full-field strain and displacement in the specimen is easily monitored by using the deformation measurement techniques. Although there are also some drawbacks worth noting in the semi-circular bending (SCB) test, such as shear failure may occur near the support roller during the test of SCB specimen without a notch [12,13], the aforementioned advantages still motivated the researchers to utilize the SCB tests to investigate and evaluate fatigue cracking properties of asphalt concrete pavement [14].

Paris law, an empirical crack growth model, was well-known and widely used to predict fatigue characteristics in engineering materials [15,16]. It is a power relationship between stress intensity factor (K_I) and crack length as described by Paris law [17], as shown in Equation (1). A fracture occurs when the K_I is equal to or larger than the critical stress intensity factor of the material (K_{IC}, also referred to as fracture toughness), and the K_{IC} is obtained as the stress intensity factor K_I at the critical load (P_c), as shown in Equation (2).

$$\frac{da}{dN} = A(\Delta K_I)^n \tag{1}$$

where a denotes crack length, mm; N denotes load cycle; A and n are Paris material parameters; and ΔK_I is the range of stress intensity factor, which is estimated by Equation (3):

$$K_{IC} = \sigma Y_{I(0.8)}\sqrt{\pi a} \tag{2}$$

where $\sigma = P_{max}/(2rt)$, P denotes the applied maximum load, r denotes the specimen radius, m; t being the specimen thickness, m; a is the notch length, m; and $Y_{I(0.8)}$ is the normalized stress intensity factor (dimensionless), $Y_{I(0.8)} = 4.782 + 1.219\left(\frac{a}{r}\right) + 0.063\exp(7.045(a/r))$.

$$\Delta K_I = K_{I(max)} - K_{I(min)} = \Delta\sigma(\pi a)^{-0.5} \tag{3}$$

where $K_{I(\max)}$ is K_I the related to the maximum stress amplitude in a half-sine load, $K_{I(\min)}$ is the K_I related to the minimum stress amplitude in a half-sine load, Δ is the difference between $K_{I(\max)}$ and $K_{I(\min)}$.

The crack length tracking throughout testing is essential to accurately determine the K_I during a test. However, a substantial challenge in the process of determining Paris law is to track the crack length change corresponding to each cycle, due to the limitation of conventional measurement methods such as strain gauges, extensometers, and linear variable differential transformers [18,19]. Therefore, instead of directly determining the crack length, researchers preferred to establish a correlation between crack length and a measurable parameter to measure the crack length. For example, the relationship between actuator displacement and crack length established by the finite element analysis method can determine the real change of the crack length [20]. Another common method for measuring the crack length is to establish the relationship between crack mouth opening displacement (CMOD) and crack length over several fatigue certain periods [21–23].

The digital image correlation (DIC) technique, which is an optical non-contact, full-field strain and displacement measurement method, is one of the alternative crack length measurement techniques that could monitor the crack length corresponding to each cycle in real-time [24–27]. Therefore, utilizing the DIC technique to monitor the crack length propagation of asphalt concrete in the fatigue test is increasingly popular in measuring Paris law parameters. For instance, the digital photographs were used to record crack length propagation of asphaltic materials during the fatigue test, thereby determining the Paris law parameters to evaluate the effect of binder grade on fatigue performance of bituminous [18]. Furthermore, the fatigue characteristics difference for asphalt concrete at various temperatures, including crack propagation, fatigue zone, and crack tip remodeling, strain distribution, could also be characterized by capturing the speckle pattern displacement variation on the surface of specimen images [28].

Albeit DIC techniques and Paris law have been widely used to characterize the fatigue and fracture properties of asphalt concrete, several gaps remain to be addressed as follows: First, using DIC technology to measure the growth of the fatigue crack length of specimen in the SCB fatigue test is not straightforward because it is time-consuming and tedious to track the crack length change from each frame of the picture [21]. Particularly, those fatigue tests with low-stress amplitude may generate tens of thousands of pictures. Second, the actual vehicle load on the road surface is constantly changing, and the Paris law parameters of the one asphalt concrete may vary under different stress ratios [29–31]. Thus, more efforts should be expended on modifying the Paris law to enable it to characterize the fatigue properties of asphalt concrete under a wide stress level range. Third, the realistic fatigue behavior of asphalt pavement is always accompanied by crack occurrence, hence the crack parameters such as crack length should be considered in evaluating and predicting the fatigue resistance of asphalt concrete. However, the current fatigue life prediction models of asphalt concrete proposed by previous literature, such as the viscoelastic continuum damage model, dissipated energy ratio, and 50% stiffness reduction [32–34], are all indirect and lack crack parameters. Therefore, it is of great interest to accurately and rapidly determine the crack growth rate during the fatigue crack propagation process for helping evaluate the fatigue resistance and formulating the utilizing strategies of the original asphalt surface layer.

2. Objectives

To overcome the abovementioned limitations, the main objectives of this paper are fourfold: (1) determination the real-time measurement method of fatigue crack length growth of asphalt concrete in corresponding to each cycle of load application; (2) evaluation the effect of stress ratio on the fatigue properties of various road sections; (3) characterization of the fatigue resistance for various road sections under a different stress ratios range using Paris law master curve; (4) estimation of the residual life of the high-performance asphalt concrete freeways with a service life of more than 20 years.

3. Materials and methodology

3.1. Basic information of pavement samples

In this paper, the asphalt concrete core specimens were drilled from the Yanjing freeway in Jiangsu province, China. Yanjing is a two-way four-lane highway that serves heavy volume traffic. It was opened to traffic in 2001, and it has been used nearly for 20 years. In China, the freeways were divided into different sections according to the integer kilometers corresponding to the mileage. For example, K84 in this manuscript represents the road section corresponding to the Yanjing freeway between 84 km and 85 km. In this paper, three road sections namely K84, K124, and K165 were employed for analysis, the basic information of three typical road sections is shown in Table 1. The performance condition index (PCI) of three road sections is above 90, indicating that these pavements' conditions are at a satisfactory level

Table 1
The basic performance indexes of typical sections.

mileage number	Road sections	Cumulative ESALs (time*10^4)	Crack length (m/Km)	Asphalt surface thickness (cm)	PCI
K84	1	385.2	87	17	97
K124	2	560.02	52	19.5	97
K165	3	679.81	12	19.3	94

[3]. However, it is inconsistent with the actual condition of pavements. For instance, the Equivalent Single Axle Load (ESALs) of section 3 is much more than section 1, suggesting that the cumulative damage and residual fatigue life of asphalt concrete of the two sections may be quite different. These traditional performance indicators neither effectively distinguish the fatigue resistance and residual life difference among different road sections, nor help the Department of Transportation (DOT) and contractors to develop the old road utilization strategies in reconstruction and expansion projects. In this regard, it is essential to develop an effective method to quantitatively evaluate the fatigue crack resistance and residual life of long-term service asphalt concrete.

The pavement structures and the maintenance history of three road sections are depicted in Fig. 1. It can be seen that the previous pavement maintenance programs (hot-in-place recycling, recovering, milling, and repaving) of three road sections mainly focused on the upper surface. The intermediate surface layer was seldom maintained during the service period. Therefore, this paper mainly focuses on the evaluation of the fracture and fatigue resistance characteristics of the middle surface layer.

This paper was organized as shown in the flowchart (Fig. 2). The SCB specimens were first drilled from three freeway road sections. Then, preliminary experiments including monotonic SCB and cyclic SCB fatigue tests subjected to various stress ratios were conducted at 15 ℃. During the tests, a DIC technique was employed to monitor the crack length, fracture and fatigue process zone, crack tip remodeling, and strain distribution on the surface of the specimens. The subsequent section elaborated using the K-d tree algorithm to automatically trace the change of crack length in DIC images corresponding to each fatigue load cycle. Meanwhile, the bilinear softening of the cohesive zone model (CZM) was used to determine the strain threshold of asphalt concrete crack to ensure the accuracy of the crack length calculated using the K-d tree algorithm. Next, the effect of stress ratios on the crack growth rate and Paris law parameters were analyzed, and then the Paris law master curve was constructed to characterize the fatigue resistance of asphalt concrete in a wide range of loads. Finally, the Paris law master curve and finite element analysis (FEA) were combined to estimate the number of load applications that road sections can withstand.

3.2. Asphalt concrete specimens' preparation

The cylindrical cores were taken from the three sections of the Yanjing freeway. The locations of drilling cores and the laboratory test procedures are presented in Fig. 3 and Fig. 4, respectively. Nine asphalt concrete cores were extracted from each section, eight cores with 150 mm diameter were used for the SCB test, and one core with 100 mm diameter was applied to measure the deep of crack.

The standard procedures for samples preparation were exhibited in Fig. 5, firstly, the specimens were cut according to the thickness of the pavement surface layer structure. Thereafter, the middle surface layer of each core was trimmed into two semi-circles (150 mm in diameter and 50 mm thick, and 15-mm-deep mechanical notch) to be used for fatigue and fracture tests of asphalt concrete. Four semi-circle specimens of each road section were used for monotonic SCB tests, and the others were used for SCB fatigue tests.

3.3. Monotonic SCB test program

The monotonic SCB test was performed according to the European standard BS EN 12697–44:2010 [35]. The UTM-25 universal testing machine (IPC Company, Australia) was employed to perform the monotonic SCB test for determining the specimen's fracture strength. As shown in Fig. 5, the load bracket consisted of a loading roller and two supporting rollers. The distance between the two supporting rollers was set to 120 mm, which was 0.8 times the specimen diameter. The specimens were loaded with a constant displacement at a rate of 50 mm/min in a three-point bending load configuration at a test temperature of 15 ℃ and the test stopped when the load dropped to 0.1 kN in the post-peak region. Four sample replicates were prepared conducted the monotonic SCB test for each road section at the same condition. The SCB tensile strength of the specimen was calculated based on Equation (4) [35]. To ensure the internal temperature of specimens is consistent with the test temperature, the specimens should be stored in a thermostat chamber with 15 ℃ for more than four hours.

$$\sigma_{max} = \frac{4.263^{*}F_{max}}{D^{*}t} \tag{4}$$

where D is the diameter of specimen, mm; t is the thickness of specimen, mm; F_{max} is the maximum force of specimen, N; 4.263 is a constant recommended by BS EN 12697–44:2010.

3.4. Cyclic SCB fatigue test program

According to the previous literature [21,36], the setting of the stress level during the fatigue test process of stress-controlled will have a significant impact on the fatigue performance of asphalt concrete. For instance, the specimens may fail due to excessive deformation, and thus the softer asphalt concrete may exhibit a relatively lower fatigue life than the asphalt concrete with high strength. To avoid this problem, this paper performed monotonous SCB tests to determine the tensile strength of specimens, and then the values of 0.2-, 0.3-, 0.4-, and 0.5-times tensile strength were separately applied as stress in SCB fatigue tests [19,37]. Three replicates for each stress level were performed under the cyclic loading condition and the variations coefficient for the fatigue life from the SCB fatigue tests should be less than 20%. The load frequency was set to 10 Hz, which was approximately corresponding to a vehicle speed of 60 km/h [12,38]. To keep the uniform contact between the specimen and the loading roller, a contact load of 0.2 kN was applied for 10 s before the actual load. The cyclic repeated compressive loads with a half-sinusoidal waveform were applied to perform the SCB fatigue test.

Fig. 1. The pavement structures and the maintenance history of three road sections.

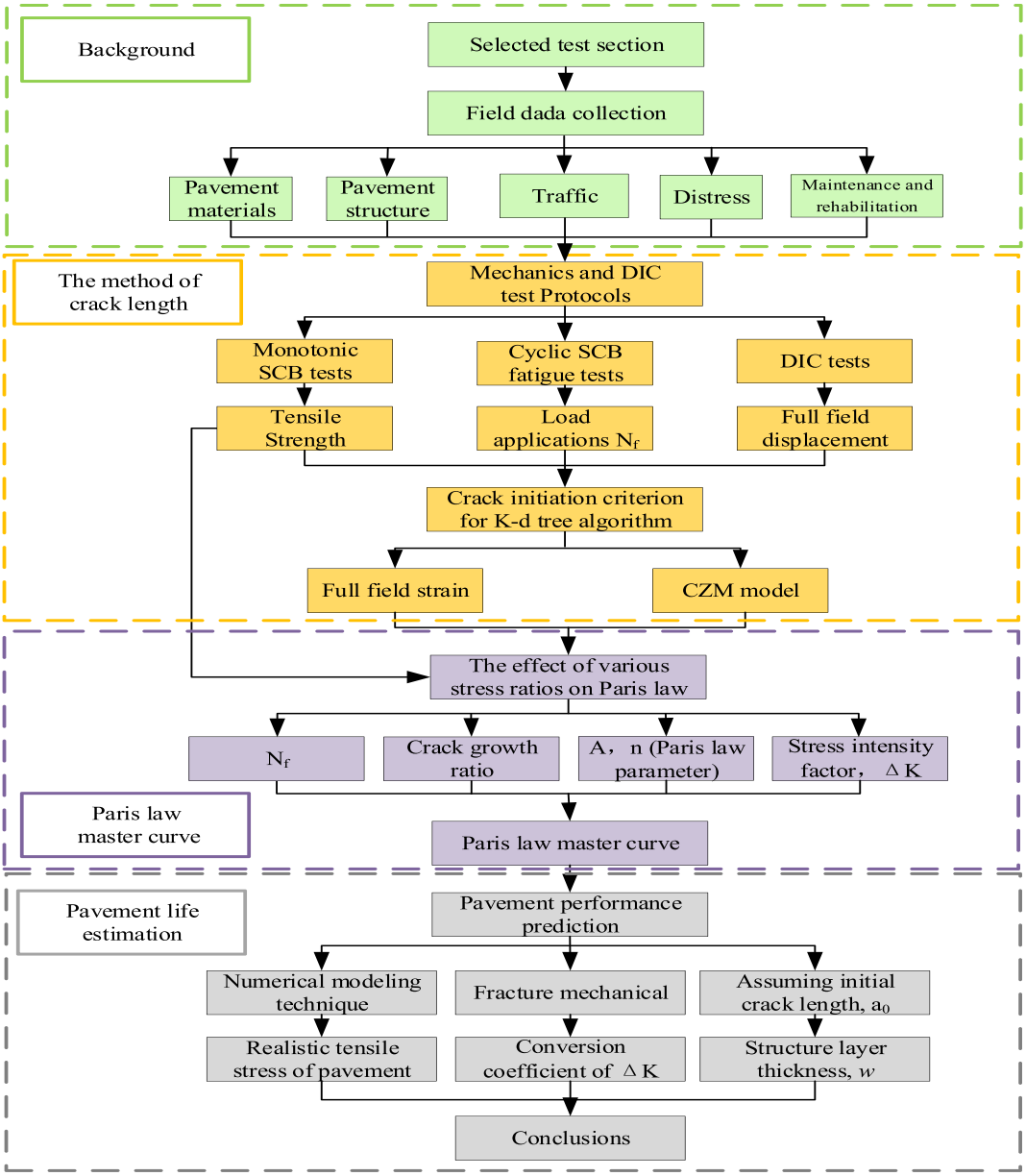

Fig. 2. Organization and flowchart of the study.

3.5. Stereo-digital image correlation techniques

Compared with the 2D-DIC using a single camera, the stereo-DIC techniques equipped with two cameras can provide more accurate strain measurements as the measured results are not affected by unavoidable out-of-plane motions [19]. As shown in Fig. 4, the specimens were firstly spray-painted using white matt paint, and then black matt paint was used to speckle the black dot onto dried white paint of the surface. Two industrial cameras, with 48 × 2048 pixels, 11.264 × 11.264 mm of optical size, and 80 fps acquisition speed, were used to record images of the front surfaces of the specimen during the test. The lighting with a 20-watt strip LED lamp was installed in the loading box to ensure a good gray range of the image even under the condition of high frame rate and low exposure time.

3.6. K-dimension tree neighbor-searching algorithm

K-d tree algorithm is a data structure divided by data points in k-dimensional space, which is mainly applied to search the key data in multi-dimensional space, such as search range and nearest neighborhood search [39]. According to known data points (training set), the K-d tree continuously divides the space into smaller and smaller regions (binary tree) to reduce the complexity of the nearest neighbor search, and then captures neighbor elements more quickly in vector quantization encoding. In this paper, the K-d tree algorithm was employed to track the change in crack length in each fatigue load cycle. The specific steps are shown in Fig. 6. Firstly, the propagation trajectory of fatigue cracks for the specimen was determined through the images of several frames before the failure of the specimen. Secondly, the propagation trajectory was manually delineated in the strain field of the specimen, and then the focus range of the strain field was narrowed to a neighborhood with a radius of 0.8 mm near the crack. Next, a natural cubic spline was used to fit the delineated curve and then discretized into dense points. For each discrete point, the strain values of its neighbors within a 0.8 mm radius in each frame of the image were retrieved. The point that reached the strain threshold for the first time in the neighborhood was determined as the crack point. Finally, the crack length corresponding to each image could be determined by calculating the

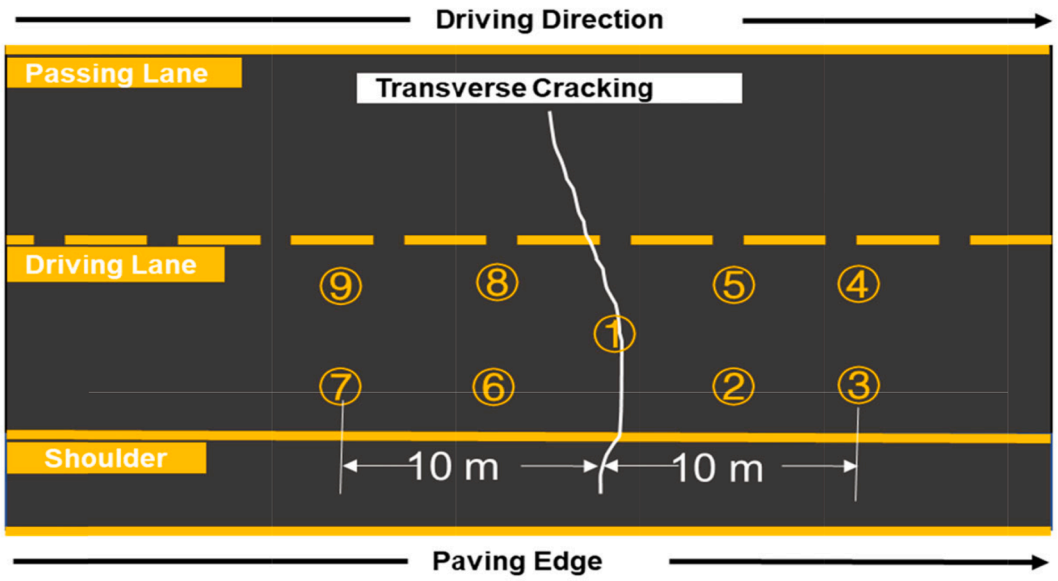

Fig. 3. Sampling location of the cores.

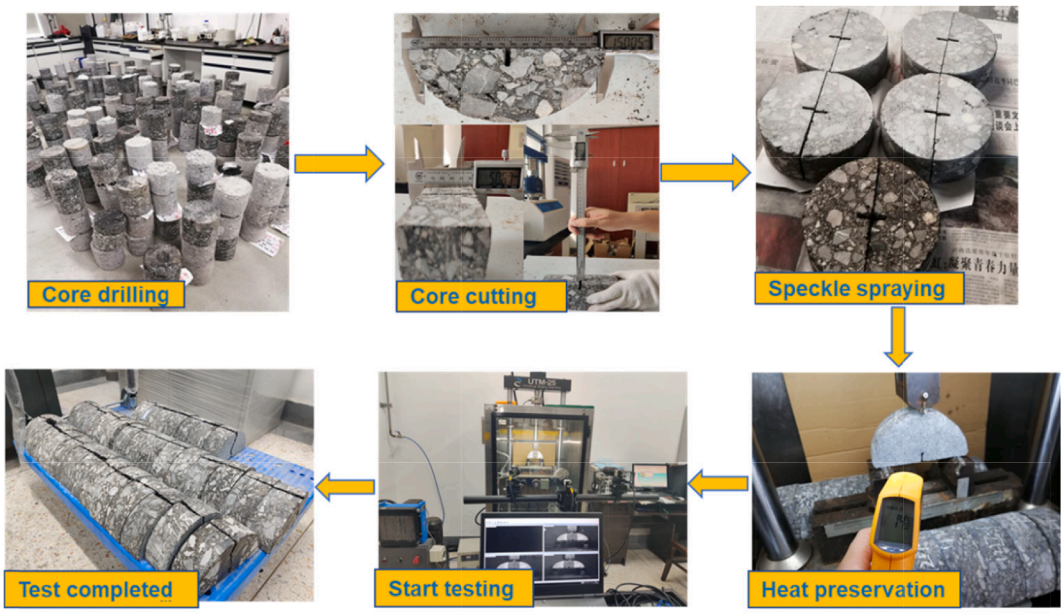

Fig. 4. Laboratory SCB test procedures.

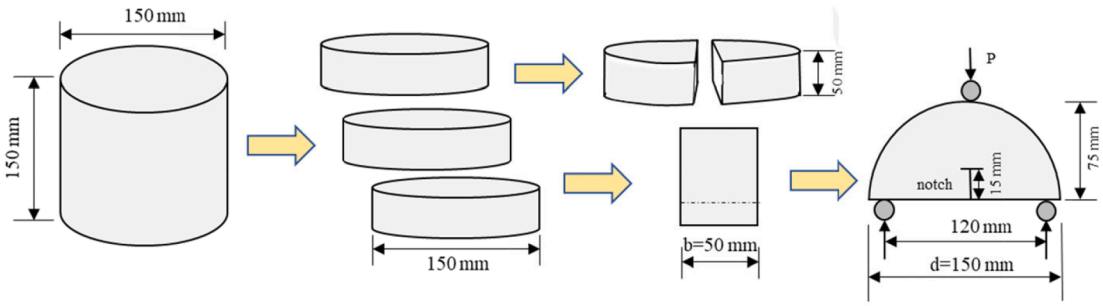

Fig. 5. The standard procedures for samples preparation.

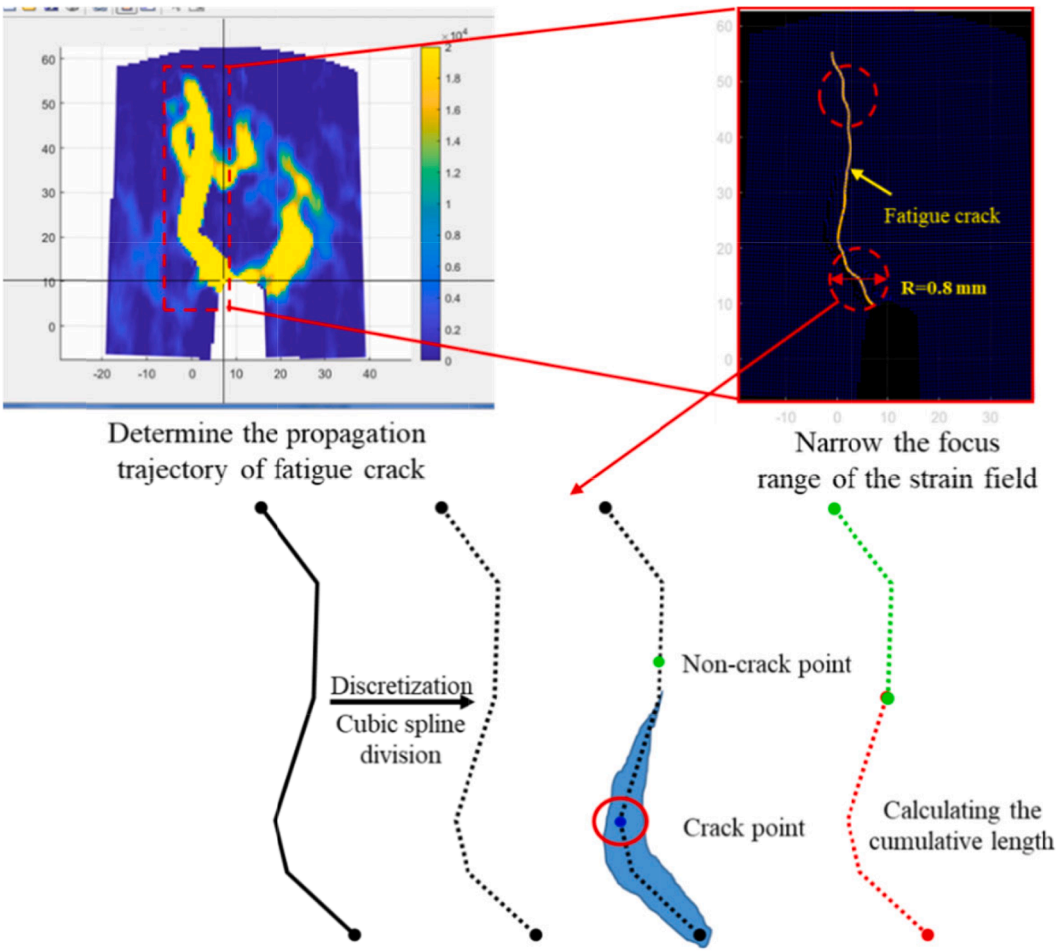

Fig. 6. Schematic diagram of the K-d tree nearest neighbor search algorithm.

cumulative length of the crack points.

The search radius of 0.8 mm was picked for the following reasons: firstly, the geometric size of the specimen was much larger than that of a pixel in the images at a resolution of 2048 × 2048. The search range and computational cost would increase with the increase of the search radius. Meanwhile, the propagation trajectory of fatigue cracks for the specimen has been tracked and recorded by the DIC technique, and thus it was unavailing to expand the radius to search for the cracking point in the area beyond the cracking trajectory. Secondly, due to the limitation of the resolution, the effective point could not be captured if the search radius is too small. The search radius of 0.8 mm was close to the geometric size (0.8 mm) of a pixel at a resolution of 2048 × 2048. Taken together, a search radius of 0.8 was picked to determine the cracking pointing.

3.7. Cohesive zone model (CZM) for crack modeling

Determining the crack strain range of specimen fatigue crack is a prerequisite to ensure the accuracy of the crack length calculated using the K-d tree nearest neighbor search algorithm. Some literature has tried to define the cracking strain range of specimens through DIC pictures and full-field strain [25,40], while these methods are somewhat arbitrary and empirical. The cohesive zone model (CZM) as an effective phenomenological model has been widely used to characterize the crack initiation and propagation in the fracture process zone (FPZ) [41]. Toward that end, this study combined the bilinear softening CZM and the general static analysis step model with the monotonic SCB test to determine the strain threshold corresponding to crack initiation of the specimen.

3.7.1. CZM with a bilinear constitutive law

The bilinear CZM concept in the fracture mode I is presented in Fig. 7 (a) and (b), where δ_n, δ_{cr}, t_n, and σ_c are the normal opening displacement, the displacement corresponding to the zero traction, the normal traction, and the material tensile strength [42].

There are three parameters in the bilinear CZM, namely, cohesive strength (t^0), critical cohesive fracture energy (G), and critical opening displacement (δ_{cr}). Among them, G and t^0 of asphalt concrete can be obtained from the SCB test. The plane local coordinate system was established with the two directions parallel and perpendicular to the cohesive interface as the coordinate axis direction and the center point of the cohesive interface as the origin. In the FPZ of plane exists a normal traction component (t_n) and a shear traction component (t_t), which respectively cause the crack opening displacement (δ_n) and sliding displacement of crack surfacing (δ_t). The areas of the curve and the abscissa in Fig. 7 (c) and (d) represent the normal G_{nc} and the tangential G_{tc}, respectively. The G_{nc} and G_{tc} can be determined by Equation (5) and Equation (6).

$$G_{nc} = \frac{1}{2} t_n^0 \delta_n^c \tag{5}$$

$$G_{tc} = \frac{1}{2} t_t^0 \delta_t^c \tag{6}$$

The second nominal stress criterion is used as the discrimination ground of the initial damage of asphalt concrete, and the discriminant conditions are as Equation (7):

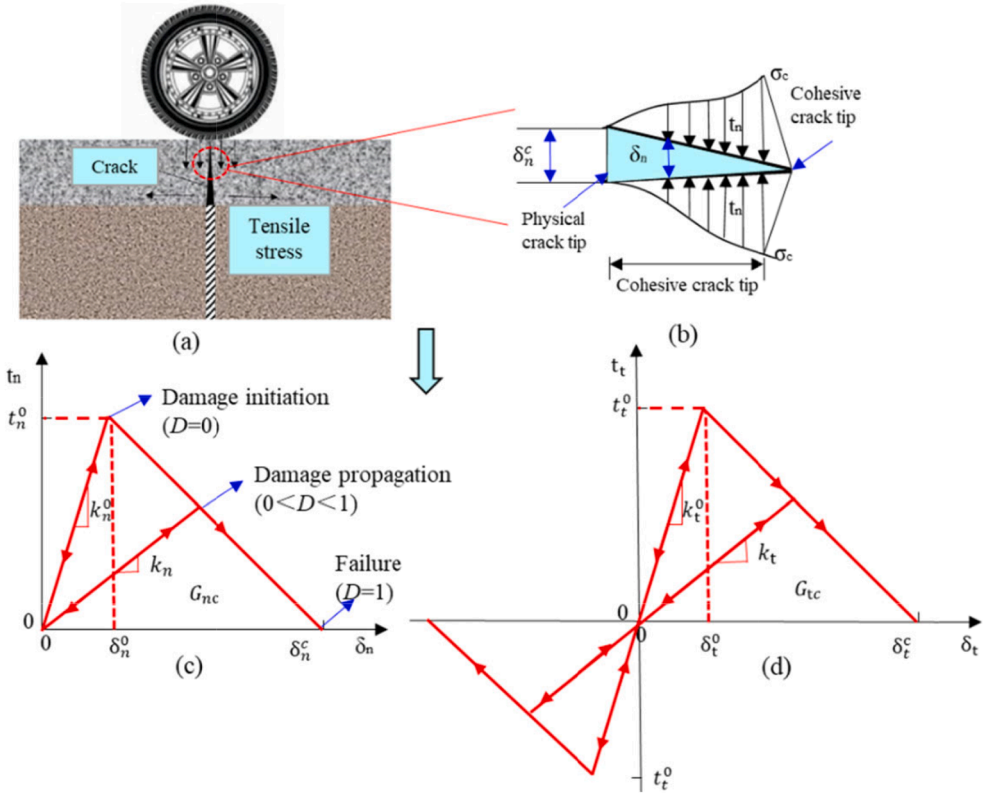

Fig. 7. Schematic illustration of typical pavement structure crack and CZM parameters in fracture.

$$\left\{\frac{\langle t_n\rangle}{t_n^0}\right\}^2+\left\{\frac{t_t}{t_t^0}\right\}^2=1 \tag{7}$$

where $<>$ is the Macaulay bracket, meaning as Equation (8):

$$\langle t_n\rangle=\begin{cases} t_n, t_n\geq 0 \\ 0, t_n<0 \end{cases} \tag{8}$$

According to the energy linear damage evolution criterion, the D is defined as a damage variable to characterize the overall damage degree of the material under t_n and t_t. The D is calculated by Equation (9):

$$\left\{\frac{G_n}{G_{nc}}\right\}^{\alpha}+\left\{\frac{G_t}{G_{tc}}\right\}^{\alpha}=D \tag{9}$$

where G_n and G_t represent the work induced by the t_n and t_t, α is the damage evolution coefficient.

The values range from 0 to 1, $D=0$, $0<D$ less than 1, and $D=1$ denote that the materials cohesive interface without damage, appearing damage and complete failure.

The normal stiffness (k_n) and tangential stiffness (k_t) attenuate when the damage appears to the cohesive interface. The relationship between the (k_n), (k_t) and the D as Equation (10) and Equation (11):

$$k_n=(1-D)k_n^0 \tag{10}$$

$$k_t=(1-D)k_t^0 \tag{11}$$

The scalar stiffness degradation (SEDG) of the cohesive zone is used to evaluate the meso-damage of SCB specimens. The SEDG can be determined by the Equation (12).

$$SEDG=\frac{k_n-k_t}{k_n} \tag{12}$$

The value of SEDG ranges from 0 to 1, $SEDG=0$ means that all elements of the cohesive model are intact; $0<SEDG<1$ suggests that some elements have been damaged but not complete failure and the elements stiffness can be restored after unloading, while the $SEDG\geq 1$ implies that some elements have been completely damaged and the elements stiffness cannot be restored.

After cohesive interface occurring damage, the relationship between t_n, t_t and δ_n, δ_t as shown in Equation (13) and Equation (14):

$$t_n=\begin{cases} (1-D)k_n^0\delta_n, & \delta_n\geq\delta_n^0 \\ k_n^0\delta_n, & \delta_n<\delta_n^0 \end{cases} \tag{13}$$

$$t_t=\begin{cases} (1-D)k_t^0\delta_t, & |\delta_t|\geqslant\delta_t^0 \\ k_t^0\delta_t, & |\delta_t|<\delta_t^0 \end{cases} \tag{14}$$

3.7.2. CZM model setups

A commercial finite element software, *ABAQUS 2020* [43], is utilized to simulate the SCB test, and the geometric size and roll position of the CZM model are consistent with the laboratory test. The material parameters of this study are given as follows: flexural tensile strength (σ) is 3.47 MPa, the G is 852 J/m^2, the Poisson's ratio is 0.25, and the E is 3500 MPa. The σ and G were measured by the monotonic SCB test results. Specifically, the σ was determined using Equation 4, while and G was obtained according to the AASHTO TP105-13. A three-node planar stress triangle element (CPS3) was used in the FEA model, and the loading roller and supporting roller were simulated by a rigid curved interface. It was assumed that the interface characteristics between the roller and specimen are frictionless hard contact. The component element and node information for the model in ABAQUS was output to the INP file, and a Python script was written to modify the INP file to realize the insertion of the cohesive force element. Finally, a modified INP file was imported into ABAQUS, the elastic properties and cohesive element properties were respectively endowed to generate the assembly.

4. Determination of strain thresholds

4.1. Effect of strain threshold on crack length measurement by K-D algorithm

As described in Section 3.6, the strain threshold of specimen crack (nominal crack strain) should be set before using the K-d tree algorithm to calculate the crack length. To determine the rational nominal crack strain for specimens, the strain thresholds were set to 200, 1000, 2000, 3000, 4000, 8000, 10000, and 20,000 με, respectively, and then the crack propagation laws corresponding to different strain thresholds are determined to compare with the crack propagation recorded in the laboratory fatigue test image, thereby roughly determining the strain threshold range of the asphalt concrete. It can be seen from Fig. 8 that except for setting stain threshold to 200 με, the fatigue crack propagation corresponding to other strain thresholds can be summarized to four stages during the cyclic SCB fatigue test, namely, the cumulative damage without cracks, the rapid growth of micro-cracks, the hold steady of crack length, and the rapid growth of macro-cracks. The strain threshold setting mainly affects the cumulative damage, the hold steady of crack length, and the rapid growth of macro-cracks stages. The setting of the strain threshold has a significant impact on the number of load cycles corresponding to each stage.

Specifically, a crack length of 20 cm was detected at the initial stage of loading when the strain threshold of the specimen was set to 200 με, which was inconsistent with the crack phenomenon observed in the test. When the strain threshold was set to 1000 με, the changing trend of the crack length with the number of load cycles increases in the first and second stages almost overlapped with that of 2000 με. Further, the change curve of the crack length with the number of load cycles increases in the third and fourth stageswhen the strain threshold elevating to 2000 με was roughly consistent with that of setting strain threshold to 3000 με. With the rise of the setting strain threshold, particularly when it exceeded 4000 με, the crack initiation time of the specimen increases significantly, the period of hold stability and failure sharply reduces, which also does not match the experimental observation results. Therefore, it was preliminarily deduced that the nominal crack strain of the specimen should be around 1000 to 3000 με.

The crack growth rate under each load cycle is directly related to A and n parameters in Paris law, as well as the stress intensity factor [44,45]. The fatigue performance of asphalt concrete can be evaluated objectively only if the change of crack length is determined accurately. Therefore, it is necessary to demonstrate the rationality of the estimated crack strain threshold of specimens through numerical simulation, thereby ensuring the accuracy of the K-d tree algorithm in calculating the crack length.

4.2. CZM calculated strain thresholds of crack initiation

A crack evolution morphology of the SCB specimen in the numerical simulation and that of in the experimental test during the loading process were shown in Fig. 9 (a) and (b), respectively. As noted, the crack propagation path calculated by the CZM model established in this study is roughly consistent with the results of DIC monitoring in a laboratory. There are three stages of the crack evolution process of asphalt concrete specimens: crack initiation, crack propagation, and fracture failure. In the first stage, a strain contour plot color of the area above the notch of the specimen goes darker as the load increases. Due to the stress concentration, the accumulated damage of the left sharp corner on the notch of the specimen increases steadily, and the micro-cracks start to appear when the stress reaches the tensile strength. At this time, the maximum strain of the specimen is about 2000 με. Afterward, the specimen turns into a crack propagation stage. The crack gradually expands upward along the mid-span section. In this phase, it can be found that when a crack expandes to the vicinity of coarse aggregate, it bypasses the aggregate and developes along with the interface between aggregate and asphalt mortar. Therefore, the crack path of the specimen is not completely upward, and it would gradually return to the vertical direction after a slight deviation. It is suggested that the distribution of coarse aggregate may change the local propagation path of crack, but may not affect the overall cracking trend.

Some differences between CZM and DIC outcomes are worth to be noted that the strain field of the CZM model can more clearly exhibit the subtle changes of strain field for the specimen, such as dozens or even several micro-strain changes, as shown from Fig. 9. However, the strain on the specimen surface would be affected by noise and not be accurately evaluated if the strain field observation scale of DIC outcomes is reduced to several hundred micro-strains. In addition, the CZM

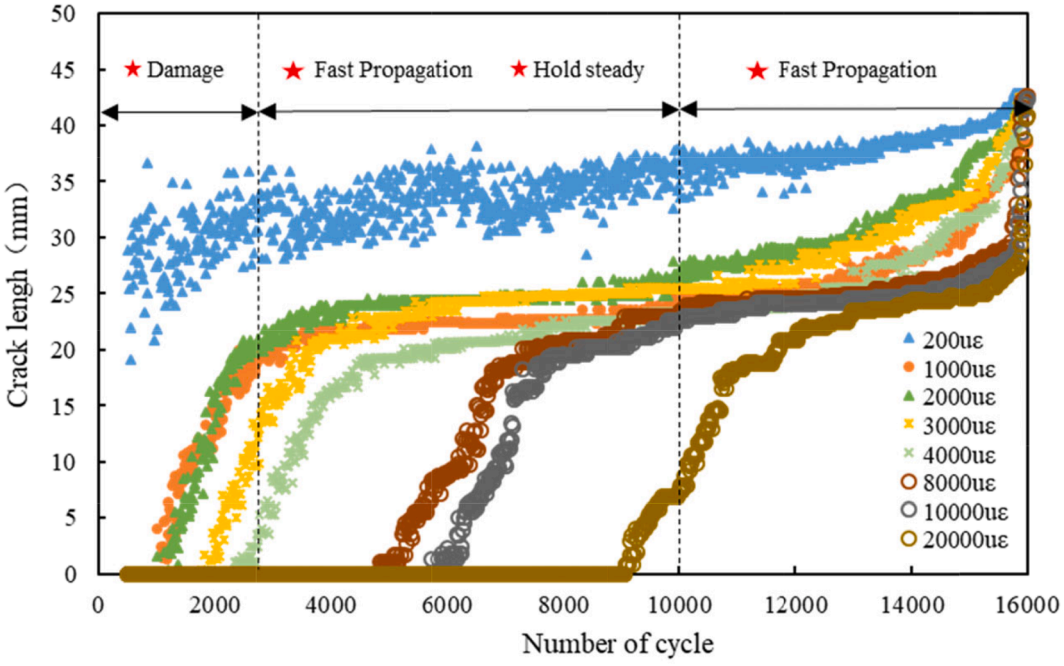

Fig. 8. The crack length calculated by K-d tree algorithm with different strain threshold.

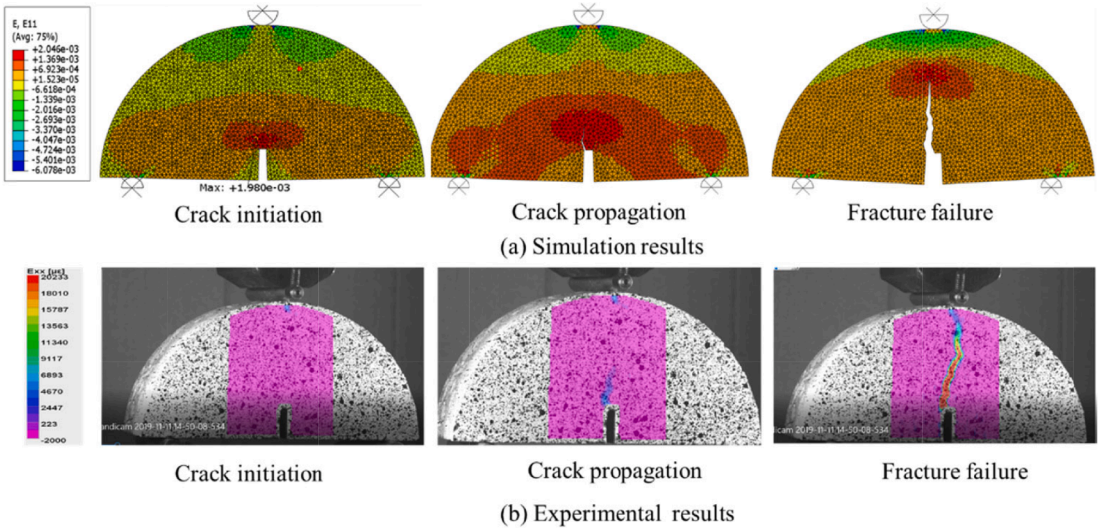

Fig. 9. Crack evolution morphology in numerical simulation and experimental tests.

outcomes can also accurately measure the strain of each element, thereby determining the nominal crack strain of asphalt concrete. In contrast, the DIC outcomes can only roughly determine a range of the nominal cracking strain for the specimen. Those differences can be attributed, at least partially, to the noise of the image collected by DIC that would lead to the calculation result of the strain field producing an error of about 200 με.

According to Fig. 10, the curve of load versus CMOD obtained by numerical simulation resembles the curve of the experimental results. Specifically, the peak load values of the simulation and experimental test are 6.07 kN and 6.02 kN, respectively. The fracture energy calculated based on the area of the load-CMOD curve obtained from the experimental test and that of simulation are 860 J/m^2 and 852 J/m^2, respectively. Results in Fig. 10 implied that the CZM model established in this paper accurately simulates the entire cracking process of the specimen.

The scalar stiffness degradation (SEDG) of the cohesive zone is a variable that can be used to characterize the extent of cohesive stiffness degradation when the damage occurs in the cohesive interface. According to the definition of SEDG in section 3.7.2, when SEDG is equal to 1, indicating that the cohesive element has been completely damaged, and the stiffness of the element cannot be restored after unloading. In this case, cracks would appear at the interface of the cohesive element. The red dot plot in Fig. 10 represents the percentage of cohesive elements with SEDG is equal to 1 (failure cohesive elements) in total cohesive elements. When the percentage of failure cohesive elements with SEDG is equal to 1 bigger than 0, meaning that micro-cracks begin to form inside the material. Hence, the nominal strain of asphalt concrete cracking initiations can be credited as the strain value corresponding to the first failure cohesive element with SEDG of 1, namely, the strain threshold for computing crack length described in Section 3.6. According to the strain contour plot of the first failure cohesive elements when the SEDG is 1, it is determined that the strain range of asphalt concrete crack initiation is about 2000 με. As shown in Fig. 10, when the applied load is less than the peak load, the percentage of failure cohesive elements with SEDG equal to 1 is always zero, which indicates that that the damage caused by the load at this time is recoverable and would not cause the asphalt concrete to crack. As the applied load reaches the peak value, the CMOD of the specimen increases rapidly, and the percentage of failure cohesive elements rapidly accumulates from zero to 0.35% and

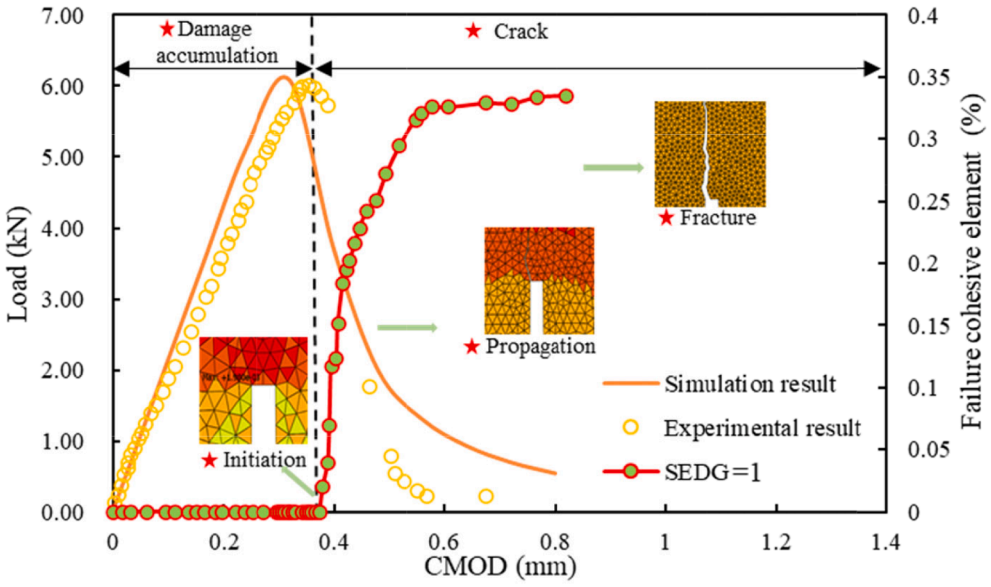

Fig. 10. Comparison of experimental test load-CMOD curve against numerical simulation load-CMOD.

eventually failure stage.

5. Results and discussion

5.1. Tensile strength of specimen

The tensile strength of the specimens for different sections at 15 ℃ and the applied stress value for the SCB fatigue test of various stress ratios are listed in Table 2. As shown in Table 2, the average value of tensile strength for K84, K124, and K165 are respectively 3.43, 3.70, and 3.81 MPa, and the average tensile strength of all the specimens is 3.64 MPa. It can be seen that the standard deviation of tensile strength for the parallel specimens for K84, K124, and K165 are respectively 0.03, 0.38, and 0.39 MPa, indicating that the dispersion degree of tensile strength parallel specimens in the same section is less than 15%.

For another, one-way analysis of variance (ANOVA), a method that could be applied to compare whether two sample means are significantly different or not, which is employed to measure the level of significance for the tensile strength between the various road sections. For a given confidence level μ (95% in this case), if the *P*-value produced by ANOVA tests exceeds 1-μ, it means that two samples are not significantly different from a statistical perspective [46]. The analysis results of one-way variance analysis are presented in Table 3. It can be seen that the P-values between the three road sections are respectively 0.2096, 0.6792, and 0.0940, indicating that the P-values between various road sections are greater than the test level of 0.05. Therefore, there is no statistically significant difference in the tensile strength of each road section.

According to the basic information of pavement samples, the performance grade of asphalt binder and gradation type used to produce asphalt concrete for various road sections were the same. Moreover, the intermediate surface layer was seldom maintained during the service period, indicating that the asphalt binders of various road sections exhibit similar aging and hardening levels. Therefore, the tensile strength of asphalt concrete in each road section is not much different at the test temperature of 15 °C.

5.2. DIC of fatigue crack growth

The top part of Fig. 11 shows the crack state of the specimen at the fatigue life stages of 20, 40, 60, and 80%N_f. Note that even if the fatigue life of the specimen reaches 40%N_f, only very limited crack propagation can be distinguished, not to mention the determination of a crack length. Only when fatigue life exceeds 80%N_f, the crack propagation stage be induced by notch tip blunting and the crack opening can be observed. In contrast, the DIC technique can track the torturous crack propagation with a frequent crack deflection, thereby identifying and measuring the crack length change of specimens at each fatigue fraction.

The middle and lower parts of Fig. 11 display the strain contours of specimens under the stress ratio of 0.3 and 0.4 of fatigue tests, respectively. The same specimen of one road section exhibits very different fatigue crack paths and localized zones at different levels of load application because of the heterogeneity of asphalt concrete specimens. Fatigue crack propagations in heterogeneous materials are complex and different mechanisms, particularly for those asphalt concretes that exhibit brittleness and hardening due to aging and vehicle loads. For instance, the crack area at the stress ratio of 0.3 is large than that of the stress ratio of 0.4, indicating that energy dissipative processes for asphalt concrete are different at various stress levels. Fig. 11 presents the localized zone propagation for the same specimen at different stress levels, which contained both the fracture process zone and the macro-crack after its onset. The maximum micro-strain determined in front of the notch tip can characterize the effect of stress level on the fatigue deformation resistance for asphalt concrete under the same fatigue periods (such as 20%N_f). Specifically, the maximum micro-strain of asphalt concrete under the stress ratio of 0.3 is always smaller than that of the stress ratio of 0.4.

It can be found that when the stress ratio is 0.3, with the increase of the number of load cycles (greater than 40%N_f), the crack tends to bridge (in which secondary cracks nucleate before the primary crack) and bifurcate (in which the primary crack branches into many sub-cracks except one of them keeps propagating others arrest when the life fractions greater than 80%N_f). The large FPZ at a crack tip can be attributed to the cracks of asphalt concrete propagating along with the interface between aggregate and asphalt mortar under low-stress ratios. Under a stress ratio of 0.4, only a tiny crack can be observed in the specimen before the primary crack initiation. As the load cycle increase, a few sub-cracks appear, and then the cracks of specimens rapidly propagate up to fracture failure. Therefore, the same asphalt concrete may present different crack propagation behaviors during SCB fatigue tests of various stress ratios. According to the discussions above, investigation of the effect of stress ratios on Paris law parameters of asphalt concrete is helpful to comprehensively evaluate the fatigue characteristics of the asphalt pavement under different load conditions.

Table 3
One-way analysis of variance.

Source of variance	SS	df	MS	F	P-value	F crit
Between section 1 and 2	0.1431	1	0.1431	1.9736	**0.2096**	5.9873
Within section	0.4350	6	0.0725			
Sum	0.5781	7				
Between section 1 and 2	0.0276	1	0.0276	0.1886	**0.6792**	5.9873
Within section	0.8780	6	0.1463			
Sum	0.9056	7				
Between section 1 and 3	0.2964	1	0.2964	3.9495	**0.0940**	5.9873
Within section	0.4503	6	0.0750			
Sum	0.7468	7				

Table 2
Result of SCB strength test and applied stress level of SCB fatigue test.

Stake number	Specime nnumber	Monotonous SCB tests				Cyclic SCB tests	
		Peak load F_{max} (kN)	Tensile strengthS (MPa)	Mean value S (MPa)	Standard deviation	Stress ratios	Stress (MPa)
K84(Section 1)	1	6.07	3.45	3.43	0.03	0.2	0.68
	2	6.12	3.47			0.3	1.03
	3	5.97	3.39			0.4	1.37
	4	6.02	3.42			0.5	1.72
K124(Section 2)	1	6.40	3.63	3.70	0.38	0.2	0.74
	2	7.39	4.20			0.3	1.11
	3	5.78	3.28			0.4	1.48
	4	6.52	3.69			0.5	1.85
K165(Section 3)	1	6.88	3.91	3.81	0.39	0.2	0.76
	2	7.45	4.23			0.3	1.14
	3	5.81	3.30			0.4	1.52
	4	6.74	3.83			0.5	1.90

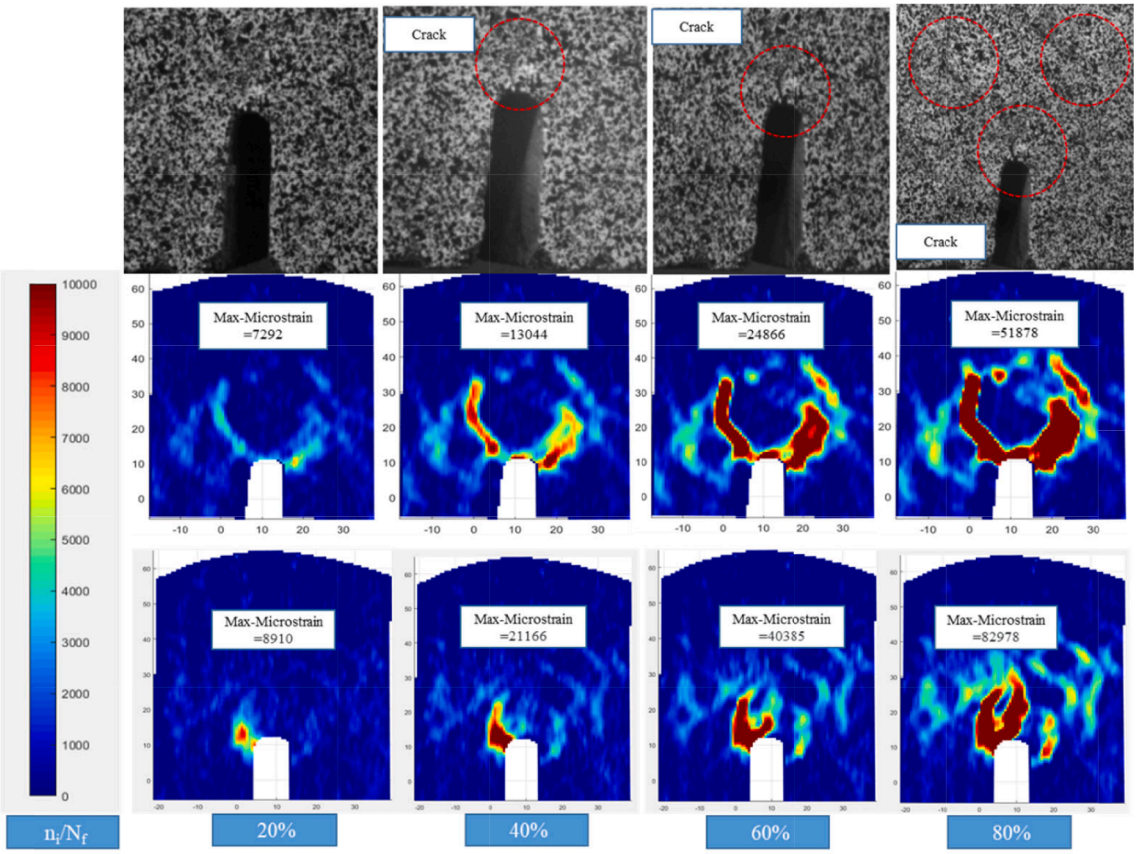

Fig. 11. The crack propagation and the DIC contours of fatigue tests at various fatigue life fractions, ni/Nf.

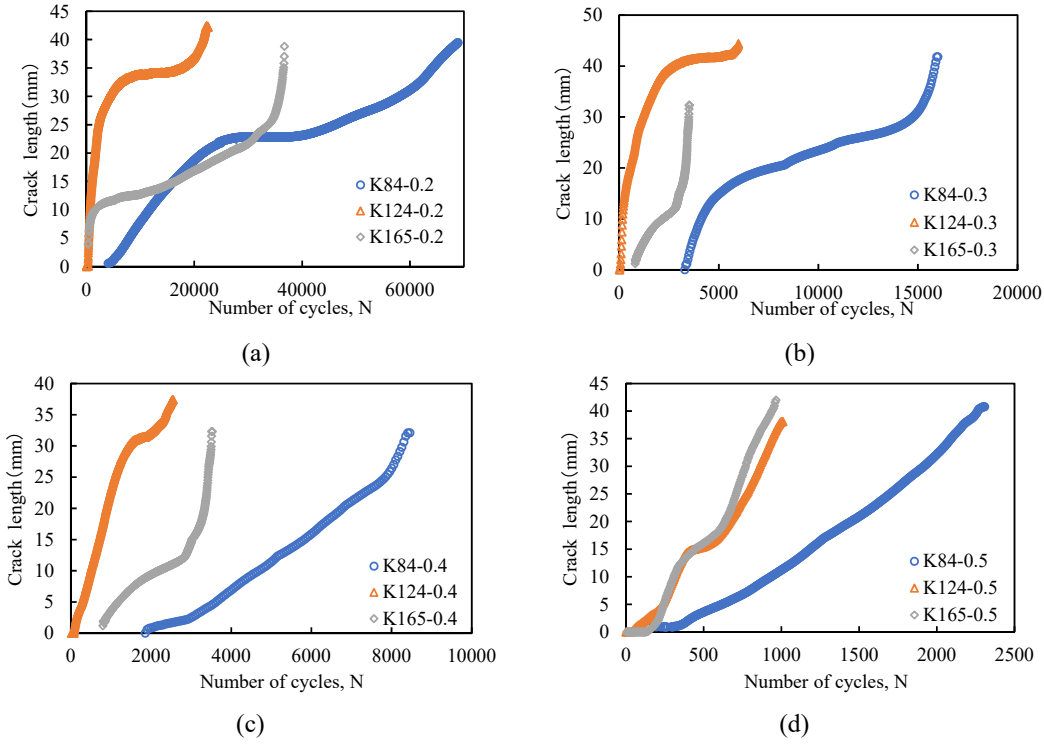

Fig. 12. Fatigue crack length versus load cycles at various stress ratios.

6. Determination of the Paris law with various stress ratios

6.1. Fatigue crack growth with various stress ratios

Although many secondary crack initiation and propagation in the FPZ ahead of the crack tip for specimen, it is generally assumed that the crack growth is dominated by a single macrocrack when utilizing fracture mechanics methods to analyze the crack criterion and fatigue behavior for asphalt concrete [18]. Therefore, only one crack change is considered in the calculation of the crack length. The crack length versus load cycles of road sections under different stress ratios was plotted in Fig. 12. A typical crack propagation process of the rock or cement concrete can be roughly divided into three stages, namely, the fast growth, hold steady growth, and fast growth in the failure stages. The proportions of the three stages in the entire life cycle are 5%-10%, 70%-85%, 15%-20% of N_f, respectively [22]. However, the corresponding cycles of the second stage for asphalt concrete drop dramatically with the increase of the stress ratio. Particularly, when the stress ratio climbs to 0.4 or 0.5, the crack length of the specimen shows a linear increasing trend. Therefore, under the low-stress ratio (0.2 or 0.3), the propagation process of fatigue crack for asphalt concrete can show pronounced three-stage characteristics. Under this scenario, the fatigue crack propagation curve follows a similar S-shaped trend, which implies that the fatigue crack propagation rate for the first stage is roughly consistent with that of the third stage. In addition, it also indicates that the fatigue crack propagation rates for both the first and third stages are greater than that of the second stage. However, the difference of the slopes and curvatures among those curves suggests that the crack propagation rate for various road sections is different even at the same fatigue crack propagation stage. For another, the crack propagation of all sections in the third stage increases rapidly, which is approximately a line in the logarithmic coordinate system of the Paris law. Furthermore, the length of secondary cracks in the specimen stops propagating when the number of load cycles exceeds 80% of N_f. Thus, this paper employed the crack length data after 80%N_f to calculate the crack growth rate and the stress intensity factor, thereby determining the Paris parameters.

Although there is almost no difference among the total crack length of the specimens under various stress ratios, the propagation trend of the crack is significantly different. These differences can be attributed, at least partially, to the distribution of large aggregates in asphalt concrete, which may cause tortuous cracking of asphalt concrete. The crack initiation and propagation always occur at the lowest energy path of materials, thus the difference in the degree of initial damage of road sections caused by the different ESALs may also lead to tortuous cracking of asphalt concrete.

6.1.1. Paris law analysis with various stress ratios

Before determining the Paris law parameters, the crack length curve should be smoothed to ensure that the crack growth rate curve does not scatter during the numerical differentiation process. Consequently, the Savitzky-Golay convolution algorithm was employed to smooth the crack growth curve by polynomial data fitting and the least square method. The smoothed crack growth curves were then numerically differentiated and plotted against the stress intensity factor (ΔK) range on double logarithmic scales. The Paris law of three typical road sections under different stress ratios was fitted (the dashed line) as shown in Fig. 13. The constant n value represents the slope of the line, which characterizes the sensitivity of the crack propagation process to applied stress. A value larger value of n value implies that even a small change in stress can induce a relatively pronounced crack growth rate. The constant A value is da/dn (crack growth rate) at a mode I ΔK range of 1 N/m$^{0.5}$.

As shown in Fig. 13 (a), with the increase of stress ratio, the n and A values of various road sections are generally show a continuous decrease and fluctuated increasing trends, indicating that the stress levels have a positive effect on the crack growth rate of asphalt concrete. When the stress ratio increases to a certain value (for example, 0.5), the specimens in each section soon enter the fatigue failure stage, and the sensitivity (n value) of the crack growth rate to the applied stress decreases sharply. Specifically, the stress ratio of 0.2, the n and A values ranking are K124 > K84 > K165 and K165 = K84 > K124, suggesting that the fatigue resistance of K124 is the best followed by K84 and K165. When the stress ratio is elevated to 0.3, the rank of fatigue resistance, *n and A* values for various road sections are consistent with that of stress ratio of 0.2. It is interesting to note that the evaluation results of the fatigue resistance of

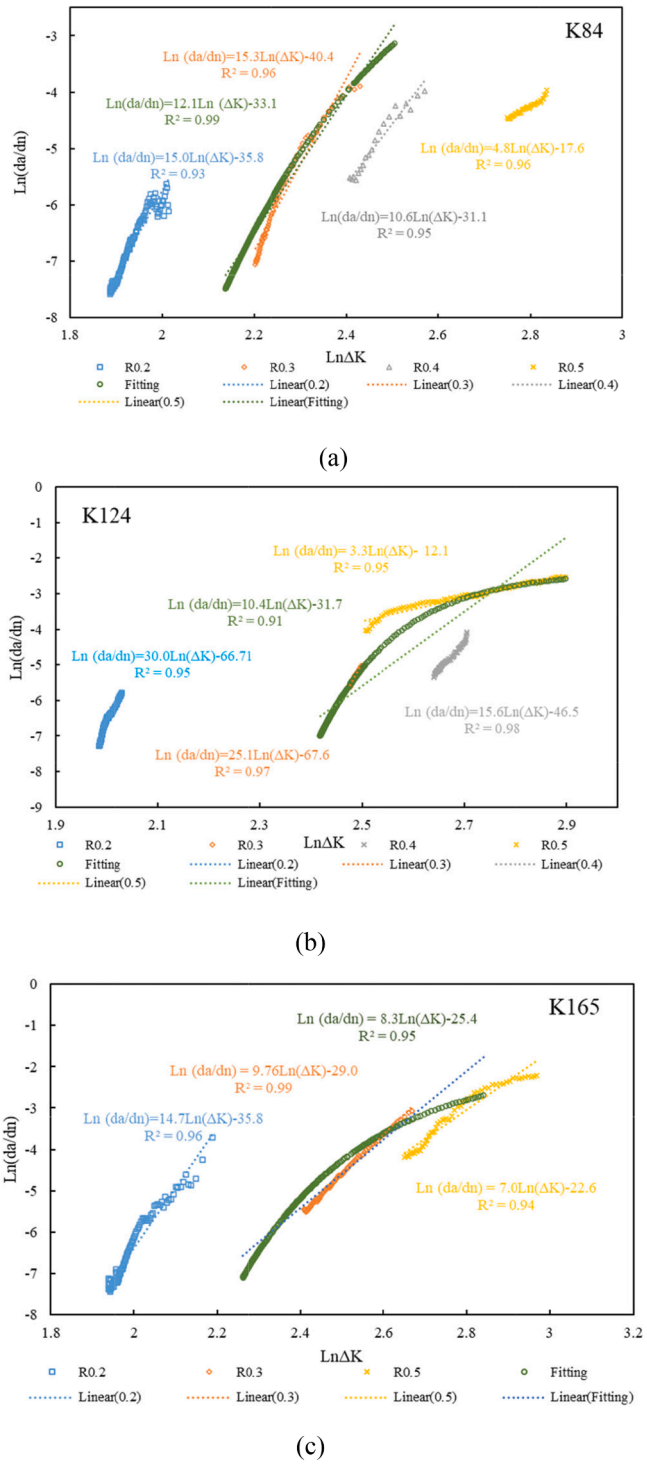

Fig. 13. Crack growth rate versus stress intensity factor with various stress ratios.

the specimens based on the A and n parameters may vary when the stress ratio further increases. For example, under a stress ratio of 0.2, the crack growth rate of K84 is greater than that of K124, while the crack growth rate of K124 is greater than that of K84 at a stress ratio of 0.5. Therefore, it is necessary to construct a comprehensive Paris law to evaluate the fatigue resistance difference of each road section within a wide load range.

6.1.2. Paris law master curve

As can be seen from Fig. 14 and Equation (3), there is a numerical equivalent relation between ΔK_I calculated when the stress level is lower and the crack length is larger (corresponding to the high cycle fatigue test of low-stress ratio) and ΔK_I calculated when the stress level is higher and the crack length is shorter (corresponding to the low cycle fatigue test of high-stress ratio). Hence, it is possible to get the same stress intensity factor under different stress ratios. This relationship among various stress ratios can be denoted by the shift factor and its calculation formula as shown in Eqs. (15) and (16). To construct a master curve, a reference stress ratio is firstly selected, and then the data collected from fatigue tests at other stress ratios are shifted to one at reference stress ratio by the shift factor. In this paper, the Sigmoid model and the nonlinear least-squares regression optimization are used to construct the master curve of the Paris law with 0.3 as the reference stress ratio. The Sigmoid model expression is shown below.

$$a(R) = \frac{\Delta K_r}{\Delta K} \tag{15}$$

$$log\left|\frac{da}{dN}\right| = \delta + \frac{a}{e^{\beta+\gamma(log\Delta K_r)}} \tag{16}$$

where $a(R)$ denotes shift factor at stress ratio (R) relative to the reference stress ratio, ΔK_r is the stress intensity factor at the reference stress ratio, ΔK is the intensity factor at tested stress ratio, α, β, δ, γ are coefficients.

The Paris law master curves of various road sections are presented in Fig. 14. The parameters (A and n) values determined by the Paris law master curve and previous literature are listed in Table 4. Although this paper used different asphalt concrete, test temperature, and load mode in fatigue test, the fracture parameters from this paper agree well with that previous literature [18,20,21], implying that the Paris law master curves constructed based on the SCB fatigue test can characterize the fatigue resistance of asphalt concrete.

The ESALs of K84 are only 3.58 million, which is lower than that of K124 and K165; hence K84 shows the slowest crack propagation rate than other road sections. The ESALs of K165 are 1.9 times that of K84 and 1.2 times that of K124, respectively. As a consequence of relatively large ESALs resulting in more serious initial damage to the middle

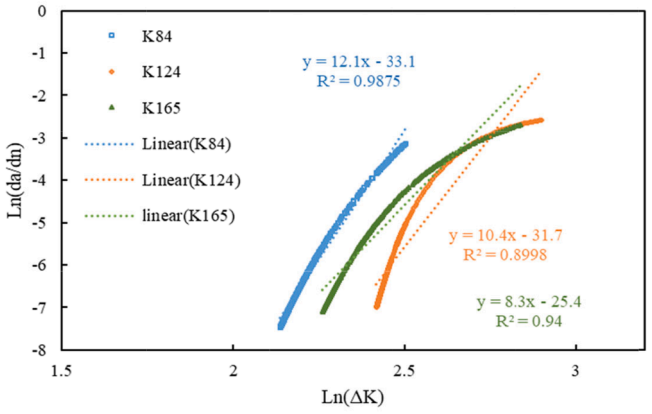

Fig. 14. The Paris law master curve at a stress ratio of 0.3 at various road sections.

Table 4
Fracture parameters of asphalt concrete.

Concrete ID	n	A	Load mode	Test temperature
K84	12.1	$4.2*10^{-15}$	SCB test	15 ℃
K124	10.4	$1.7*10^{-14}$		
K165	8.3	$9.3*10^{-12}$		
Literature 26	0.8–3.0	$2.7*10^{-12}$-$1.5*10^{-7}$	SCB test	21 ℃
Literature 25	2.7–3.9	$7.0*10^{-7}$-$1.3*10^{-3}$	SCB test	25 ℃
Literature 23	1.0–6.8	$1.2*10^{-9}$-$8.4*10^{-47}$	Compact tension test	10-30℃

surface layer of K165, the crack propagation rate of the K165 specimen is faster than K124 and K84. The fatigue load cycle of K165 is less than 200 at a stress ratio of 0.5, thus the SCB fatigue test data with this stress ratio is not used in the construction of the Paris law master curve. Macro damage of asphalt concrete, with crack initiation or propagation, occurs when the ΔK is equal to or greater than a threshold level, otherwise, it was treated as microdamage that appears to be healable after the resting period. The threshold level of the K124 is 2.41 $N/m^{-0.5}$, which is the highest of all road sections, followed by K165 and K84. The excellent fatigue crack resistance of K124 under heavy load traffic can be attributed to the fact that the total thickness of the asphalt concrete layer of K124 is the largest in these road sections. Although the results of the master curve of the Paris law have made a significant contribution to the investigation and evaluation of the fatigue properties for long-term service asphalt concrete pavement, most of the above conclusions are qualitative. It is difficult for DOT to make the utilization stratages of old pavement from the perspective of the residual life. Therefore, it is also necessary to evaluate the residual life of the middle surface layer in the road sections according to the fitting results of the Paris law master curve.

6.2. Estimation of pavement residual life

The number of load cycles required for the crack to propagate through the middle surface layer in the realistic pavement can be calculated by rearranging and integrating Eq, (1) into Eq, (17).

$$N_f = \frac{1}{A}\int_{a_0}^{w}\frac{da}{\Delta K_1^n} \tag{17}$$

where w is the thickness of the middle layer, a_0 is the initial crack length.

To determine the stress intensity factor (K_1) in Eq,(17), the maximum tensile stress of the middle surface layer bottom was firstly calculated by a numerical modeling technique, as shown in Fig. 15. Specifically, a standard wheel load of 100 kN was applied to the pavement surface on a 302 mm diameter circular contact area (simulating a super single tire), and the corresponding mechanical response was calculated at the middle surface layer bottom under the load center area. The material properties of each layer structure of pavement are listed in Table 5. As demonstrated by literature [11,18], the stress state of the asphalt concrete layer is similar to that of a bending beam or plate when the pavement layer structure is subjected to a vehicle load. Consequently, if the bending moment or maximum tensile stress at the middle layer bottom can be determined, the crack propagation can be approximately deemed to be a plate in-plane strain with a crack growth from one edge toward another side. In this case [47], a geometric factor coefficient (as shown in (18)) should be multiplied when calculating the pavement stress intensity factor. Finally, the stress intensity factor in the middle surface layer of realistic pavement can be expressed by (19)

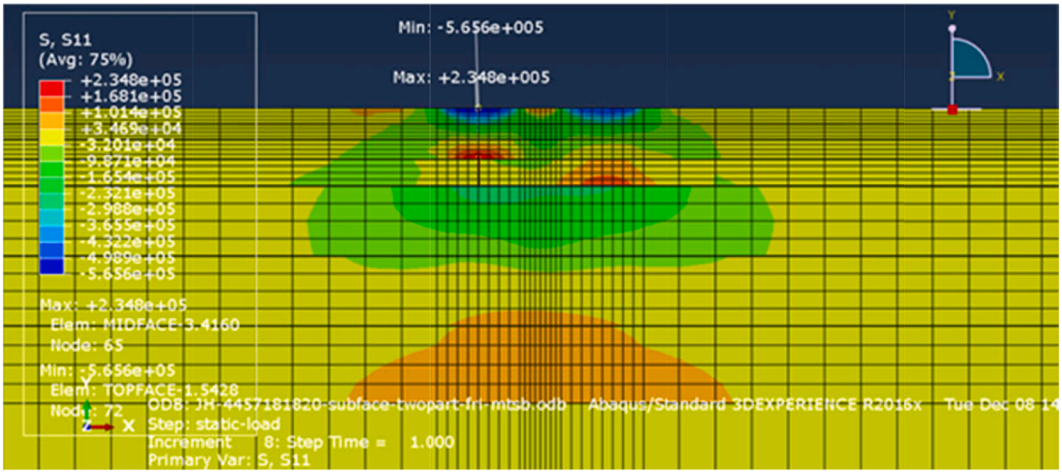

Fig. 15. Theoretically horizontal tensile stress contour of middle surface layer.

Table 5
The material properties of each layer structure of the pavement.

Layers	Moduli/MPa	Poisson's ratio
Cover layer	1400	0.25
Surface layer	1500	0.25
Middle layer	1300	0.25
Lower layer	1200	0.25
Stabilized gravel	1500	0.25
Stabilized soil	1000	0.25
Subgrade	80	0.4

$$f\left(\frac{a}{w}\right)=\frac{6\sqrt{2tan\left(\frac{\pi}{2w}\right)}}{cos_{\frac{\pi}{2w}}}\left\{0.923+0.199\left[1-sin\left(\frac{\pi a}{2W}\right)\right]^4\right\} \tag{18}$$

$$K_1=\sigma\sqrt{\pi a}F\left(\frac{a}{w}\right) \tag{19}$$

where a denotes crack length, σ denotes maximum tensile due to the bending moment, w is the thickness of the middle layer.

Assuming an initial crack length of 1 mm [11,18], the number of standard axles load (residual life) from crack initiation to travel through the entire middle surface can be estimated by numerical integration of Eq, (17). As shown in Fig. 16, the estimated load cycles to failure of K84, K124 and, K165 are 2.13E + 08, 3.57E + 08, and 1.02E + 07, respectively. It can be speculated that the primary factors affecting the residual life of pavement in this paper are: 1) the initial damage degree of the pavement, and 2) the thickness of asphalt concrete. The former factor can be characterized by the Paris law parameter, while the latter factor can be reflected by the stress level of pavement at the load action. The load cycles that the middle layer of K84 and K124 can withstand are more than 200 million, which indicates that the residual life of the middle layer in these two sections meets the requirements of the design life of the long-life pavement. Therefore, only the upper layer of K84 and K124 needs to be restored in the reconstruction and expansion project. The middle surface layer of K165 can withstand the residual load cycle of 1.02E + 07, which is less than 200 million. Therefore, it is necessary to conduct milling and resurface or increase the thickness of the pavement to meet the design standards of long-life pavement in the reconstruction and expansion project.

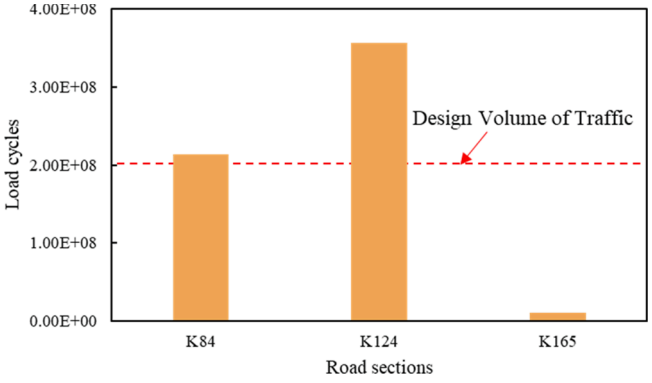

Fig. 16. The estimated residual life of the pavemen.

7. Conclusions

To determine the fatigue resistance and residual life of long-term service freeways, the stereo DIC and CZM modeling techniques were used to evaluate the crack initiation and propagation in the fatigue SCB testing. The Paris law master curve was constructed based on fatigue crack propagation law at a wide load range and the Sigmoid model to estimate the number of load applications that each section can withstand. The main conclusions are as follows:

- In the process of using the K-d tree algorithm to determine the crack length of the asphalt concrete, the larger the strain threshold was, the longer the loading period was at the crack initiation stage, and the shorter the loading period was at the hold stable stage and rapid growth stage.
- The peak load value, fracture energy, and load versus CMOD curve of the numerical simulation were roughly consistent with that of experimental results. The strain threshold of crack initiation was about 2000 με based on the strain contour plot of the first failure cohesive elements when the SEDG was equal to 1.
- The stress intensity factor threshold, *A* and *n* of Paris law parameters for asphalt concrete exhibited various change trends with the stress ratio increases. The evaluation results of the fatigue resistance of the asphalt concrete based on the Paris law parameters may vary when the stress ratio further increases.
- The Paris law master curve constructed based on the rates of fatigue crack at different stress ratios can characterize the fatigues resistance of asphalt at a wide load range. The residual fatigue life of the middle surface layer of K84, K124 and, K165 was 2.13E + 08, 3.57E + 08, and 1.02E + 07, respectively. Except for K165, other road sections meet the design expectation of the perpetual pavement that requires.

In the future, the random evolution process of the asphalt concrete damage zone will be defined by monitoring the change of the strain field area in the fatigue test, and the fatigue performance of the asphalt

concrete will be evaluated from the perspective of energy. Then, assessment viscoelastic effects developing in the asphalt concrete during the fatigue test based on DIC strain and displacement measurements. In addition, the CZM computational model is combined with the virtually generating random asphalt concrete microstructure algorithm to evaluate the effect of the aggregate and air voids on the crack propagation process and repartition of damage in the material. It will be great of great help to further explain the mechanism of fatigue cracking for asphalt concrete.

Declaration of Competing Interest

The authors declare that they have no known competing financial interests or personal relationships that could have appeared to influence the work reported in this paper.

Acknowledgement

The authors gratefully acknowledge the financial support provided by the National Natural Science Foundation of China under grant numbers (51778142), the China Civil Aviation Science and Technology Innovation Fund (MHRD20140215), and Graduate Research and Innovation Projects of Jiangsu Province under grant number (KYCX20_0128).

References

[1] Q. Dong, X. Chen, H. Gong, Performance Evaluation of Asphalt Pavement Resurfacing Treatments Using Structural Equation Modeling, Journal of Transportation Engineering, Part B: Pavements 146 (1) (2020) 04019043.
[2] P. Polaczyk, Y. Ma, R. Xiao, W. Hu, X. Jiang, B. Huang, Characterization of aggregate interlocking in hot mix asphalt by mechanistic performance tests, Road Materials and Pavement Design 22 (sup1) (2021) S498–S513.
[3] L. Zhou, F. Ni, Y. Zhao, Evaluation Method for Transverse Cracking in Asphalt Pavements on Freeways, Transportation Research Record: Journal of the Transportation Research Board 2153 (1) (2010) 97–105.
[4] M.T. Nguyen, H.J. Lee, J. Baek, Fatigue Analysis of Asphalt Concrete under Indirect Tensile Mode of Loading Using Crack Images, J. Test. Eval. 41 (1) (2013), 104589.
[5] V.M. Garcia, A. Miramontes, J. Garibay, I. Abdallah, G. Carrasco, R. Lee, S. Nazarian, Alternative methodology for assessing cracking resistance of hot mix asphalt mixtures with overlay tester, Road Materials and Pavement Design 18 (sup4) (2017) 388–404.
[6] M. Fakhri, E. Haghighat Kharrazi, M.R.M. Aliha, Mixed mode tensile – In plane shear fracture energy determination for hot mix asphalt mixtures under intermediate temperature conditions, Eng. Fract. Mech. 192 (2018) 98–113.
[7] A.M. Hartman, M. Gilchrist, Evaluating four-point bend fatigue of asphalt mix using image analysis, J. Mater. Civ. Eng. 16 (1) (2004) 60–68.
[8] S. Shen, Dissipated Energy Concepts for HMA Performance Fatigue and Healing, University of Illinois at Urbana-Champaign, 2006.
[9] G. Saha, K.P. Biligiri, Fracture properties of asphalt mixtures using semi-circular bending test: A state-of-the-art review and future research, Constr. Build. Mater. 105 (2016) 103–112.
[10] K.P. Biligiri, S. Said, H. Hakim, Asphalt Mixtures' Crack Propagation Assessment using Semi-Circular Bending Tests, Int. J. Pavement Res. Technol. 5 (4) (2012).
[11] I.M. Lancaster, H.A. Khalid, Crack propagation in the cyclic semi-circular bending test, Proceedings of the Institution of Civil Engineers - Construction Materials 167 (4) (2014) 191-200.
[12] J. Jiang, F. Ni, Q. Dong, Y. Zhao, K. Xu, Fatigue damage model of stone matrix asphalt with polymer modified binder based on tensile strain evolution and residual strength degradation using digital image correlation methods, Measurement 123 (2018) 30–38.
[13] Z. Zhou, X. Gu, J. Jiang, F. Ni, Y. Jiang, Fatigue cracking performance evaluation of laboratory-produced polymer modified asphalt mixture containing reclaimed asphalt pavement material, Constr. Build. Mater. 216 (2019) 379–389.
[14] B. Doll, H. Ozer, J.J. Rivera-Perez, I.L. Al-Qadi, J. Lambros, Investigation of viscoelastic fracture fields in asphalt mixtures using digital image correlation, Int. J. Fract. 205 (1) (2017) 37–56.
[15] G. Saha, K.P. Biligiri, Stato-dynamic response analyses through semi-circular bending test: Fatigue life prediction of asphalt mixtures, Constr. Build. Mater. 150 (2017) 664–672.
[16] G. Saha, K.P. Biligiri, Comprehensive Fatigue Mechanism of Asphalt Mixtures: Synergistic Study of Crack Initiation and Propagation, J. Mater. Civ. Eng. 30 (3) (2018).
[17] P. Paris, F. Erdogan, A critical analysis of crack propagation laws, (1963).
[18] A.C. Collop, A.J. Sewell, N.H. Thom, Laboratory assessment of the resistance to crack propagation in high-stiffness asphaltic materials, Proceedings of the Institution of Mechanical Engineers Part L Journal of Materials Design & Applications 218(1) (2004) 55-66.
[19] F. Yuan, L. Cheng, X. Shao, Z. Dong, L. Zhang, G. Wu, X. He, Full-field measurement and fracture and fatigue characterizations of asphalt concrete based on the SCB test and stereo-DIC, Eng. Fract. Mech. 235 (2020).
[20] B. Huang, S. Xiang, Z. Gang, Using notched semi circular bending fatigue test to characterize fracture resistance of asphalt mixtures, Eng. Fract. Mech. 109 (3) (2013) 78–88.
[21] J. Zhang, M. Sakhaeifar, D.N. Little, A. Bhasin, Y.-R. Kim, Characterization of Crack Growth Rate of Sulfur-Extended Asphalt Mixtures Using Cyclic Semicircular Bending Test, J. Mater. Civ. Eng. 30 (12) (2018).
[22] L. Wen, X. Shi-lang, L. Qing-hua, Theorical and experimental study on fatigue crack propagation law of ultra-high toughness cementitious composite, Engineering Mechanics 30 (11) (2013) 67–74.
[23] J. Zhang, J. Teixeira, D.N. Little, Y.R. Kim, Prediction of fatigue crack growth behavior of chemically stabilized materials using simple monotonic fracture test integrated with computational cohesive zone modeling, Compos. B Eng. 200 (2020), 108367.
[24] Y. Dai, D. Gruber, H. Harmuth, Determination of the fracture behaviour of MgO-refractories using multi-cycle wedge splitting test and digital image correlation, J. Eur. Ceram. Soc. 37 (15) (2017) 5035–5043.
[25] S.A. Safavizadeh, Y.R. Kim, DIC Technique to Investigate Crack Propagation in Grid-Reinforced Asphalt Specimens, J. Mater. Civ. Eng. 29 (6) (2017).
[26] C. Li, L. Wang, X.X. Wang, Crack and crack growth behavior analysis of asphalt mixtures based on the digital speckle correlation method, Constr. Build. Mater. (2017).
[27] B. Birgisson, A. Montepara, E. Romeo, R. Roncella, R. Roque, G. Tebaldi, An optical strain measurement system for asphalt mixtures, Mater. Struct. 42 (4) (2008) 427–441.
[28] C.M. Stewart, E. Garcia, Fatigue crack growth of a hot mix asphalt using digital image correlation, Int. J. Fatigue 120 (2019) 254–266.
[29] T. Mann, The influence of mean stress on fatigue crack propagation in aluminium alloys, Int. J. Fatigue 29 (8) (2007) 1393–1401.
[30] J.K. Musuva, J.C. Radon, The effect of stress ratio and frequency on fatigue crack growth, Fatigue Fract. Eng. Mater. Struct. 1 (4) (2007) 457–470.
[31] A. Ohta, E. Sasaki, M. Kosuge, Effect of Stress Ratios on the Fatigue Crack Propagation Rate, Transactions of the Japan Society of Mechanical Engineers 43 (373) (1977) 3179–3191.
[32] B.S. Underwood, A continuum damage model for asphalt cement and asphalt mastic fatigue, Int. J. Fatigue 82 (JAN.PT.3) (2016) 387–401.
[33] A.H. Abedali, Fatigue performance predication model based on dissipated energy criteria using DSR under controlled-strain mode, Innovative Infrastructure, Solutions 3 (2018) 23.
[34] G.M. Rowe P. Blankenship T. Bennert,and AASHTO Standard Specifications, Fatigue Assessment of Conventional and Highly Modified Asphalt Materials with ASTM and AASHTO Standard Specifications, Fatigue Assessment of Conventional and Highly Modified Asphalt Materials with ASTM 2012.
[35] E. 12697–44, Bituminous Mixtures-Test Methods for Hot Mix Asphalt Part 44: crack Propagation by Semi-Circular Bending Test 2010 European Committee for Standardization Brussels Belgium.
[36] A. Margaritis, G. Jacobs, G. Pipintakos, J. Blom, Fatigue Resistance of Bituminous Mixtures and Mortars Containing High Reclaimed Asphalt Content, Materials 13 (24) (2020) 5680.
[37] Z. Zhou, X. Gu, F. Ni, Q. Li, X. Ma, Cracking resistance characterization of asphalt concrete containing reclaimed asphalt pavement at intermediate temperatures, Transp. Res. Rec. 2633 (1) (2017) 46–57.
[38] S. Lv, C. Liu, D. Chen, J. Zheng, Z. You, L. You, Normalization of fatigue characteristics for asphalt mixtures under different stress states, Constr. Build. Mater. 177 (2018) 33–42.
[39] V. Ramasubramanian, K.K. Paliwal, Fast k-dimensional tree algorithms for nearest neighbor search with application to vector quantization encoding, IEEE Trans. Signal Process. 40 (3) (1992) 518–531.
[40] B. Hill, W.G. Buttlar, Evaluation of polymer modification in asphalt mixtures through digital image correlation and performance space diagrams, Constr. Build. Mater. 122 (2016) 667–673.
[41] Y. Zhao, F. Ni, L. Zhou, L. Gao, Three-dimensional fracture simulation of cold in-place recycling mixture using cohesive zone model, Constr. Build. Mater. 120 (2016) 19–28.
[42] E.V. Dave, B. Behnia, Cohesive zone fracture modelling of asphalt pavements with applications to design of high-performance asphalt overlays, Int. J. Pavement Eng. 19 (3) (2017) 319–337.
[43] ABAQUS2020, [Computer software], Dassault Systèmes, Providence, RI.
[44] H. Li, X. Luo, Y. Zhang, R. Xu, Stochastic fatigue damage in viscoelastic materials using probabilistic pseudo J-integral Paris' law, Eng. Fract. Mech. 245 (2021), 107566.
[45] H. Li, X. Luo, Y. Zhang, A kinetics-based model of fatigue crack growth rate in bituminous material, Int. J. Fatigue 148 (2021), 106185.
[46] D. Howell, Statistical Methods for Psychology, J. Roy. Stat. Soc. 43 (43) (2012).
[47] T.L. Anderson, Fracture mechanics: fundamentals and applications, CRC press2017.